IEEE Access
Multidisciplinary | Rapid Review | Open Access Journal

Received November 6, 2019, accepted November 20, 2019, date of publication November 25, 2019,
date of current version December 10, 2019.

Digital Object Identifier 10.1109/ACCESS.2019.2955379

Transient Modeling and Analysis of VSC Based DC Microgrid During Short Circuit Fault

HENG NIAN, (Senior Member, IEEE), AND LIANG KONG
College of Electrical Engineering, Zhejiang University, Hangzhou 310027, China

Corresponding author: Heng Nian (nianheng@zju.edu.cn)

This work was supported by the National Key Research and Development Program of China under Grant 2017YFB0903300.

ABSTRACT The application of distributed renewable energy (DER) drives the development of DC microgrid based on voltage source converter (VSC). And short circuit fault protection is a significant challenge for the development of VSC based DC microgrid. This paper proposes a transient modeling method for VSC based DC microgrid. Firstly, the transient characteristics of VSC under DC bus voltage control mode and active power control mode are analyzed. And then the faulty DC microgrid model, which consists of VSC model and DC line model, is modeled. And the calculation expressions of state variables in DC microgrid are presented. Next, the correctness of proposed modeling approach is verified by comparing with the electromagnetic transient (EMT) simulation by Matlab/Simulink. Moreover, the case study on the parameters configuration of DC microgrid protection devices shows that the transient modeling method can be effectively used in faulty DC microgrid analysis. The method proposed in this paper can not only ensure the calculation efficiency, but also improve the accuracy of DC microgrid analysis on fault.

INDEX TERMS DC microgrid, dc fault, voltage source converter (VSC), dc bus voltage control mode, active power control mode.

I. INTRODUCTION

The voltage source converter (VSC) based DC microgrid is a promising concept in power system whose transmission scale is smaller than high-voltage DC (HVDC) transmission system [1]. Firstly, there are no concepts of phase and reactive power in DC microgrid. Thus phase synchronization of generation units and reactive power compensation are not needed to be considered in DC microgrid control system [2], [3]. Secondly, The control method of VSC is flexible so that VSC can change the flow direction of power transmission to meet the flexible and adjustable requirements of connection of distributed energy resources (DER) [4], [5]. Therefore, compared with traditional AC distribution gird, VSC based DC microgrid is more suitable to incrementally connect DER to power grid [6]–[8].

Since the line impedances in DC microgrid are lower than that in traditional AC grid, all the bus capacitors discharge rapidly and the DC lines generate overcurrent when the short circuit fault occurs in DC microgrid [9]. Thus, the short circuit fault protection is a non-ignorable challenge in VSC based DC microgrid. In order to achieve the fault detection, protection design and parameters tuning, it is necessary to accurately obtain the transient characteristic of VSC based DC microgrid on short circuit fault [10]. There have been preliminary studies on DC grid fault analysis. In [11], the transient characteristic of a DC pole-to-pole fault is analyzed under the consideration of the injected power from AC grid and the model of DC grid is derived. In [12], fault before IGBT blocked is analyzed in detail, and the model of DC grid on the pole-to-pole short circuit fault is also derived. In [10], a simplified RLC MMC model is given and then a general calculation model of faulty current in complex DC grid (including radial type and looped type topology) is established.

VSC operates as a power interface in DC microgrid to link with AC grid and DER [13]. In existing studies, there are two ways to develop the current model outputted from VSC in faulty DC grid. The first way is to regard the VSC as constant current source (CCS), which is used in [11]. The other way is to ignore the current from VSC, which is mainly used in [10]. However, with the development of semiconductor devices, VSC switching frequency is increased and control period may be shortened within 0.1ms [14]. Since protection devices, i.e. circuit breaker (CB), need several milliseconds to detect and break the faulty line in VSC based DC microgrid [10],

The associate editor coordinating the review of this manuscript and approving it for publication was Zhilei Yao.

the output current of VSC will response dynamically with the transient characteristic of faulty VSC based DC microgrid. The error of those two ways, which regards VSC as CCS or ignores the current from VSC, becomes non-negligible. Thus it is necessary to model and analyze the transient characteristic of VSC for the faulty DC microgrid model.

When the short circuit fault occurs in the VSC based DC microgrid, VSC will keep the intrinsic control mode until the fault protection is activated [15], [16]. Thus the influence of closed loop controller on the transient characteristic of VSC has to be considered in the transient modeling. However, there are still several difficulties in the transient modeling of VSC [17], [18]. Firstly, the control strategies of VSC are mainly consisted of the constant DC voltage control and constant power control, and different control strategies will cause the different transient response. Secondly, many factors such as parameters of controllers, output limitation of current controllers and the electromagnetic transient relationship between input and output of control system, will influence the VSC modeling. Thirdly, there exists the coupling between the transient response of VSC and faulty DC microgrid, thus the transient voltage and current in DC line of faulty DC microgrid should be considered in the transient modeling of VSC.

Under this situation, based on the transient model of VSC with the different control modes, a transient modeling method for VSC based DC microgrid is proposed in this paper. The main contributions of the proposed transient modeling method can be described as following: 1) The transient response of VSC under DC bus voltage control and active power control on faulty DC microgrid is analyzed and modelled; 2) An transient modeling and analysis method of faulty DC microgrid which combines VSC modeling and DC line modeling is proposed.

The rest of this paper is organized as follows, Section II analyzes VSC modeling in DC microgrid. And the difference of transient response of VSC under DC bus voltage control and active power control is pointed out. Section III presents transient modeling and analysis method of faulty VSC based DC microgrid. The proposed modeling method of VSC based DC microgrid is validated in Section IV. Section V draws the conclusion.

II. TRANSITENT CHARACTERISTICS OF VSC IN DC MICROGRID

The VSC works as a power interface in DC microgrid to link with AC grid. In this Section, the circuit topology of VSC based DC microgrid is given. And the different transient characteristics of VSC under DC bus voltage control mode and active power control mode are analyzed.

A. CIRCUIT TOPOLOGY

The VSC topology and its connection with DC microgrid are shown in FIGURE 1. P_{ac} is active power from AC grid to DC microgrid. U_s is voltage of AC grid, U_c is AC side voltage of VSC, U_{dc} is DC side voltage of VSC. i_{dc} is current from VSC to bus capacitor. i_{dco} is current from bus capacitor to DC microgrid. X_{ac} is converter reactance.

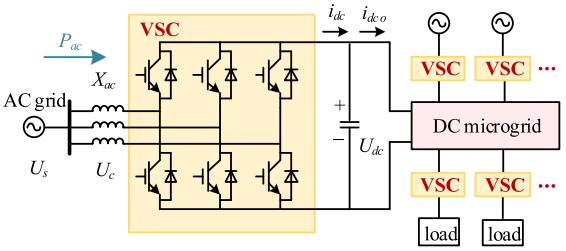

FIGURE 1. VSC based DC microgrid schematic diagram.

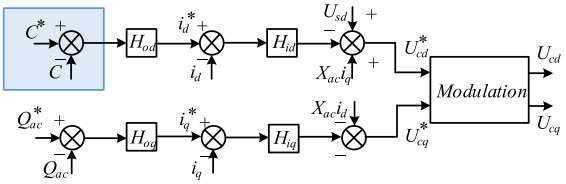

FIGURE 2. Double closed loop control diagram.

B. RESPONSE ANALYSIS OF VSC ON FAULT

As the power interface between DC microgrid and AC grid, VSC has several optional control strategies. Two main control methods are normally employed in VSC, i.e., DC bus voltage control mode and active power control mode [19]. DC bus voltage control is used to stabilize DC bus voltage, while active power control is used to regulate active power transmission between DC microgrid and AC grid. On the other hand, no matter what the control method is employed in VSC, the double closed loop control is the most commonly used control diagram in VSC, as shown in FIGURE 2.

The controllers in VSC control system are assumed to adopt PI controller and the outputs U_{cd}^* and U_{cq}^* can be expressed as:

$$\begin{cases} U_{cd}^* = U_{sd} - H_{id} \cdot (i_d^* - i_d) + X_{ac} i_q \\ \qquad = U_{sd} - H_{id} \cdot (H_{od} \cdot (C^* - C) - i_d) + X_{ac} i_q \\ U_{cq}^* = -H_{iq} \cdot (i_q^* - i_q) - X_{ac} i_d \\ \qquad = -H_{iq} \cdot (H_{oq} \cdot (Q_{ac}^* - Q_{ac}) - i_q) - X_{ac} i_d \end{cases} \tag{1}$$

where C is U_{dc} when DC bus voltage control is used, while C is active power P_{ac} when active power control is used. Q_{ac} is reactive power. i_d and i_q are d-q axis current respectively. U_{cd} and U_{cq} are d-q axis voltage of U_c respectively. U_{sd} are d-axis component of U_s. H_{od}, H_{oq} are outer loop controller of d-q axis respectively. H_{id}, H_{iq} are inner loop controller of d-q axis respectively.

According to [20], when the output of current controllers lowers than the limitation ($U_c^* \le U_{dc}/\sqrt{3}$), the relationship

between U_{cd}, U_{cq}, U_{cd}^* and U_{cq}^* can be expressed as:

$$\begin{cases} U_{cd} = U_{cd}^* \\ U_{cq} = U_{cq}^* \end{cases} \tag{2}$$

When the output of current controllers hits the limitation, the relationship between U_{cd}, U_{cq}, U_{cd}^* and U_{cq}^* can be expressed as:

$$\begin{cases} U_{cd} = U_{cd}^* \cdot \dfrac{U_{dc}}{\sqrt{3}} \cdot \dfrac{1}{\sqrt{(U_{cd}^*)^2 + (U_{cq}^*)^2}} \\ U_{cq} = U_{cq}^* \cdot \dfrac{U_{dc}}{\sqrt{3}} \cdot \dfrac{1}{\sqrt{(U_{cd}^*)^2 + (U_{cq}^*)^2}} \end{cases} \tag{3}$$

In order to analyze the transient voltage and current characteristic of DC grid under short circuit fault, the two control modes for VSC should be analyzed as follows.

1) DC BUS VOLTAGE CONTROL

DC bus capacitor discharge and U_{dc} drops when short circuit fault occurs in VSC based DC microgrid. The outer loop reference C is U_{dc} when DC bus voltage control is used in VSC. Since U_{dc} decreases, U_{cd}^* is decreases according to (1). However, due to the bandwidth of the control loop, the DC bus voltage still cannot be maintained at the reference value. Thus, DC bus voltage keeps dropping after fault occurs.

Meanwhile, the active power P_{ac} from AC grid to DC microgrid can be expressed as:

$$P_{ac} = U_{sd} \cdot i_d + U_{sq} \cdot i_q \tag{4}$$

Since i_d increases as i_d^* increases, P_{ac} keeps increasing after fault occurs.

2) ACTIVE POWER CONTROL

When active power control is used in VSC, all inputs of control system (P_{ac}, Q_{ac}, i_d and i_q) are AC side variables of VSC. And those inputs can be expressed as:

$$\begin{cases} P_{ac} = (U_s \cdot U_c / X_{ac}) \sin\delta \\ Q_{ac} = U_s \cdot (U_s - U_c \cos\delta)/X_{ac} \\ i_d = (U_{sd} - U_{cd} + X_{ac} i_q)/R \\ i_q = (U_{sq} - U_{cq} - X_{ac} i_d)/R \end{cases} \tag{5}$$

where δ is the angle between U_s and U_c, R is resistance of converter reactor.

According to (1)(5), U_c and the inputs of VSC are dynamically balanced in steady state. When fault occurs in VSC based DC microgrid, the dynamic balance continues before the output of current controllers hits the limitation. Otherwise,U_c starts to decreases according to (3). The dynamic balance on the AC side is broken and P_{ac} increases.

Meanwhile, since the DC bus voltage is not regulated directly in active power control, the DC bus voltage drops and the dropping rate is greater than that under DC bus voltage control.

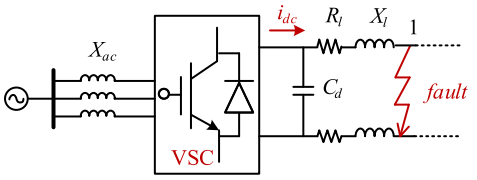

FIGURE 3. Transient model of VSC under short circuit fault.

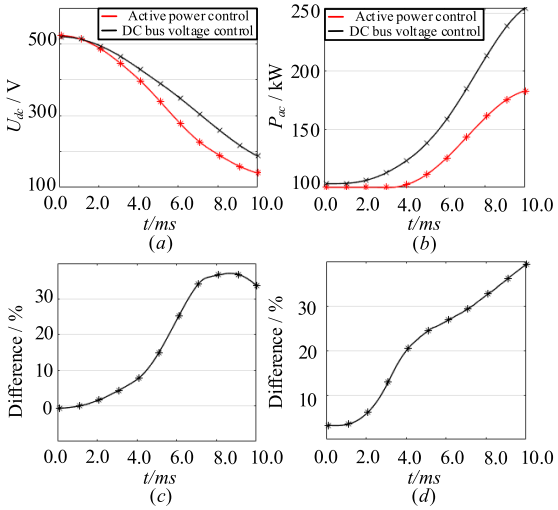

FIGURE 4. Comparison of two different control strategies: (a) comparison of DC bus voltage, (b) comparison of active power, (c) difference of DC bus voltage, (d) difference of active power.

3) COMPARISON OF TWO DIFFERENT CONTROL STRATEGIES

In order to analyze the difference of the model under two control strategies, a VSC simulation model is established by Matlab/Simulink as shown in FIGURE 3. DC bus capacitance C_d is set as 8000μF. Line resistance R_l is set as 0.24Ω. Line inductance X_l is set as 1.8mH. Converter reactance X_{ac} is set as 2mH. The AC voltage is set as 380V. The DC voltage is set as 522V under DC bus voltage control. The active power is set as 100kW under active power control.

When pole-to-pole fault occurs at the point 1 in FIGURE 3, the value and difference of DC bus voltage and active power under two different control strategies after the short-circuit fault occurs are shown as FIGURE 4.

The value of DC bus voltage under two different control strategies is shown as FIGURE 4 (a). And the difference of DC bus voltage under two different control strategies is shown as FIGURE 4 (c). Both the voltages under two control strategies keep decreasing after fault occurs. Since the drop rate of DC bus voltage under active power control is faster than that under DC bus voltage control, the difference under two control strategies grows rapidly within 7ms. And the difference reaches to 35% at 7ms. Since the drop rates of DC bus voltage under two control strategies are basically the same from 7ms to 10ms, the difference remains around 35% after 7ms.

The active power from AC grid to DC microgrid under two different control strategies is shown as FIGURE 4 (*b*). And the difference of active power is shown as FIGURE 4 (*d*). The simulation of active power under active power control is same to the theoretical analysis. Since the output of current controllers lowers than the limitation within 3ms, the active power under active power control keeps steady while that under DC bus voltage control increases gradually. And the difference under two control strategies reaches to 13% at 3ms. Since active power under active power control rises slower than that under DC bus voltage control from 3ms to 10ms, the difference keeps increasing after 3ms. Finally, the difference almost reaches to 40% at 10ms.

Therefore, it can be found that the different transient characteristic of VSC with two different control strategies will occur under short circuit fault of VSC based DC microgrid. And this different transient characteristic needs to be considered in transient modeling of VSC based DC microgrid.

III. TRANSIENT MODEL OF DC MICROGRID

In this Section, a transient model of faulty VSC based DC microgrid, which is divided into VSC modeling and DC line modeling, is modeled. Especially the VSC model is modeled and verified under DC bus voltage control and active power control respectively.

Note that the mainly application of the transient model is to achieve the fault detection, protection design and parameters tuning in DC microgrid. It means that the detection plus opening time of the CB is the selection reference of simulation time. Since the detection plus opening time of CB in DC microgrid is less than 10ms [21]–[24], all simulations only until 10ms in this paper.

A. TRANSIENT MODELING METHOD OF VSC BASED DC MICROGRID

FIGURE 5 shows the schematic diagram of modeling method for VSC based DC microgrid. The modeling method is divided into VSC modeling (including control system modeling and output-input modeling) and DC line modeling. Control system modeling is aimed to obtain the model of VSC control system including the inner current controller and outer power/DC voltage controller. While output-input modeling of VSC is aimed to obtain the output response (P_{ac}, Q_{ac}, i_d and i_q) with the input U_{cd} andU_{cq}. DC line modeling will obtain the relationship of line current and node voltage in VSC based DC microgrid. Meanwhile, U_{dc} and i_{dc} are the links between VSC modeling and DC line modeling. By combining the above three parts, the transient characteristics of VSC based DC microgrid after fault can be obtained.

Note that the main purpose to analysis the transient characteristic of VSC based DC microgrid on short circuit fault is aimed to achieve the fault detection, protection design and parameters tuning. Since the value of DC bus voltage is higher than zero during this period, this paper does not discuss the diode freewheeling stage after dc bus voltage drops to zero.

B. VSC TRANSIENT MODELING UNDER DC BUS VOLTAGE CONTROL

1) CONTROL SYSTEM MODELING

The *s*-domain expression of PI controllers can be expressed as:

$$H_\alpha(s) = K_{p\alpha}(1 + \frac{1}{s\tau_{i\alpha}}) \tag{6}$$

where H_α represents PI controller H_{od}, $H_{oq}H_{id}$ and H_{iq}respectively, $K_{p\alpha}$ is proportional coefficients in PI controller, $\tau_{i\alpha}$ is integral time constants in PI controller.

Based on the *s*-domain expression of PI controllers, the *s*-domain expressions of U^*_{cd} and U^*_{cq} can be expressed as:

$$\begin{cases} U^*_{cd}(s) = -H_1(s)\cdot H_2(s)\cdot (U_{ref}(s) - U_{dc}(s)) \\ \qquad\qquad +H_2(s)\cdot I_d(s) + U_s(s) + X_{ac}I_q(s) \\ U^*_{cq}(s) = -H_3(s)\cdot H_4(s)\cdot (Q_{ref}(s) - Q_s(s)) \\ \qquad\qquad +H_4(s)\cdot I_q(s) - X_{ac}I_d(s) \end{cases} \tag{7}$$

where U_{ref} is reference of DC bus voltage, Q_{ref} is reference of reactive power.

Substituting (6) into (7), U^*_{cd} and U^*_{cq} can be expressed as:

$$\begin{cases} U^*_{cd}(s) = \left[-K_{p1}\cdot K_{p2}\cdot A\cdot (U_{ref}(s) - U_{dc}(s))\right] \\ +\left[K_{p2}\cdot \dfrac{s\tau_{i2}+1}{s\tau_{i2}}\cdot I_d(s)\right] + \left[U_s(s) + X_{ac}I_q(s)\right] \\ U^*_{cq}(s) = \left[-K_{p3}\cdot K_{p4}\cdot B\cdot (Q_{ref}(s) - Q_s(s))\right] \\ +\left[K_{p4}\cdot \dfrac{s\tau_{i4}+1}{s\tau_{i4}}\cdot I_q(s)\right] + \left[-X_{ac}I_d(s)\right] \end{cases} \tag{8}$$

where

$$\begin{cases} A = \dfrac{\tau_{i1}\tau_{i2}s^2 + (\tau_{i1}+\tau_{i2})s + 1}{\tau_{i1}\tau_{i2}s^2} \\ B = \dfrac{\tau_{i3}\tau_{i4}s^2 + (\tau_{i3}+\tau_{i4})s + 1}{\tau_{i3}\tau_{i4}s^2} \end{cases} \tag{9}$$

In order to analyze transient characteristics of VSC, the time domain expressions of U^*_{cd} and U^*_{cq} need to be obtained. However, it is difficult to obtain the time domain expressions of (8) by inverse Laplace transformation. Thus (8) is converted to the *z*-domain expressions, and then the inverse *z* transformation is used to obtain the difference equation expressions from *z*-domain expressions. Using bilinear transformation method, the *z*-domain expressions of $U^*_{cd}(z)$ and $U^*_{cq}(z)$ can be expressed as:

$$\begin{cases} U^*_{cd}(z) = u_{cd1}(z) + u_{cd2}(z) + u_{cd3}(z) \\ U^*_{cq}(z) = u_{cq1}(z) + u_{cq2}(z) + u_{cq3}(z) \end{cases} \tag{10}$$

where

$$\begin{cases} u_{cd1}(z) = -K_{p1}\cdot K_{p2}\cdot (U_{ref}(z) - U_{dc}(z))\cdot \\ \left(\dfrac{\tau_{i1}\tau_{i2}k^2 + (\tau_{i1}+\tau_{i2})k + 1}{\tau_{i1}\tau_{i2}k^2} + \dfrac{2 - 2\tau_{i1}\tau_{i2}k^2}{\tau_{i1}\tau_{i2}k^2}z^{-1}\right. \\ \left. + \dfrac{\tau_{i1}\tau_{i2}k^2 - (\tau_{i1}+\tau_{i2})k + 1}{\tau_{i1}\tau_{i2}k^2}z^{-2}\right)/(1 - 2z^{-1} + z^{-2}) \\ u_{cd2}(z) = K_{p2}\cdot \dfrac{(1 + k\tau_{i2}) + (1 - k\tau_{i2})z^{-1}}{k\tau_{i2} - k\tau_{i2}z^{-1}}\cdot I_d(z) \\ u_{cd3}(z) = U_s(z) + X_{ac}I_q(z) \end{cases} \tag{11}$$

$$\begin{cases} u_{cq1}(z) = -K_{p3} \cdot K_{p4} \cdot (Q_{ref}(z) - Q_s(z)) \cdot \\ (\dfrac{\tau_{i3}\tau_{i4}k^2 + (\tau_{i3} + \tau_{i4})k + 1}{\tau_{i3}\tau_{i4}k^2} + \dfrac{2 - 2\tau_{i3}\tau_{i4}k^2}{\tau_{i3}\tau_{i4}k^2} z^{-1} \\ + \dfrac{\tau_{i3}\tau_{i4}k^2 - (\tau_{i3} + \tau_{i4})k + 1}{\tau_{i3}\tau_{i4}k^2} z^{-2}) / (1 - 2z^{-1} + z^{-2}) \\ u_{cq2}(z) = K_{p4} \cdot \dfrac{(1 + k\tau_{i4}) + (1 - k\tau_{i4})z^{-1}}{k\tau_{i4} - k\tau_{i4}z^{-1}} \cdot I_q(z) \\ u_{cq3}(z) = -X_{ac} I_d(z) \end{cases}$$
$$k = 2/T \tag{12}$$

Through shifting theorem and translation theorem in inverse z transformation, each output component of $U^*_{cd}(z)$ and $U^*_{cq}(z)$ can be transformed to difference equation respectively.

The difference equation of $U^*_{cd}(z)$ and $U^*_{cq}(z)$ are the superposition of all output components. And the difference equation can be express as:

$$\begin{cases} U^*_{cd}(n) = u_{cd1}(n) + u_{cd2}(n) + u_{cd3}(n) \\ U^*_{cq}(n) = u_{cq1}(n) + u_{cq2}(n) + u_{cq3}(n) \end{cases} \tag{13}$$

where

$$\begin{cases} u_{cd1}(n) = -K_{p1} \cdot K_{p2} \cdot [\dfrac{\tau_{i1}\tau_{i2}k^2 + (\tau_{i1} + \tau_{i2})k + 1}{\tau_{i1}\tau_{i2}k^2} \cdot \\ (U_{ref} - U_{dc}(n)) + \dfrac{2 - 2\tau_{i1}\tau_{i2}k^2}{\tau_{i1}\tau_{i2}k^2} \cdot \\ (U_{ref} - U_{dc}(n-1)) + \dfrac{\tau_{i1}\tau_{i2}k^2 - (\tau_{i1} + \tau_{i2})k + 1}{\tau_{i1}\tau_{i2}k^2} \cdot \\ (U_{ref} - U_{dc}(n-2))] + 2u_{cd1}(n-1) - u_{cd1}(n-2) \\ u_{cd2}(n) = K_{p2} \cdot [\dfrac{1 + k\tau_{i2}}{k\tau_{i2}} \cdot i_d(n) + \dfrac{1 - k\tau_{i2}}{k\tau_{i2}} \cdot i_d(n-1)] \\ + u_{cd2}(n-1) \\ u_{cd3}(n) = U_s(n) + X_{ac} i_q(n) \end{cases} \tag{14}$$

$$\begin{cases} u_{cq1}(n) = -K_{p3} \cdot K_{p4} \cdot [\dfrac{\tau_{i3}\tau_{i4}k^2 + (\tau_{i3} + \tau_{i4})k + 1}{\tau_{i3}\tau_{i4}k^2} \cdot \\ (Q_{ref} - Q_s(n)) + \dfrac{2 - 2\tau_{i3}\tau_{i4}k^2}{\tau_{i3}\tau_{i4}k^2} \cdot \\ (Q_{ref} - Q_s(n-1)) + \dfrac{\tau_{i3}\tau_{i4}k^2 - (\tau_{i3} + \tau_{i4})k + 1}{\tau_{i3}\tau_{i4}k^2} \cdot \\ (Q_{ref} - Q_s(n-2))] + 2u_{cq1}(n-1) - u_{cq1}(n-2) \\ u_{cq2}(n) = K_{p4} \cdot [\dfrac{1 + k\tau_{i4}}{k\tau_{i4}} \cdot i_q(n) + \dfrac{1 - k\tau_{i4}}{k\tau_{i4}} \cdot i_q(n-1)] \\ + u_{cq2}(n-1) \\ u_{cq3}(n) = -X_{ac} i_d(n) \end{cases} \tag{15}$$

Through the above transformation, the difference equation of U^*_{cd} and U^*_{cq} can be finally obtained. According to (14)(15), the values of U_{dc}, Q_s, u_{cd1}, u_{cq1} at past two moment are needed in iteration of VSC variables. And the values of i_d, i_q, u_{cd2}, u_{cq2} at past moment are needed.

After fault occurs, the control system outputs U^*_{cd} and U^*_{cq} increase rapidly and even may exceed the maximum regulation limitation of the VSC. In the practical situation of VSC, the fundamental voltage of VSC is limited when VSC is over modulation, in which U^*_{cd} and U^*_{cq} need to be fixed by (3). And the control system output U_{cd} and U_{cq} after modulation can be obtained.

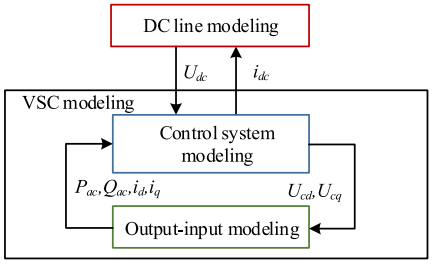

FIGURE 5. Schematic diagram of modeling method.

2) OUTPUT-INPUT MODELING

Output-input modeling is the link in transient modeling of VSC based DC microgrid. According to FIGURE 5, U_{cd}, U_{cq} are obtained from control system while P_{ac}, Q_{ac}, i_d, i_q are the outputs of output-input model.

In order to analyze VSC transients, the average modeling is used and U_{cd}, U_{cq}, i_{dc} are regard as continuous variables in this paper. According to [25], the expressions of P_{ac}, Q_{ac}, i_d, i_q and i_{dc} can be expressed as:

$$\begin{cases} P_{ac}(n+1) = U_{sd}(n) \cdot i_d(n) \\ Q_{ac}(n+1) = -U_{sd}(n) \cdot i_q(n) \\ i_d(n+1) = i_d(n) + \dfrac{\omega h}{X_{ac}} [X_{ac} i_q(n) - R i_d(n) \\ \qquad + U_{sd}(n) - U_{cd}(n)] \\ i_q(n+1) = i_q(n) + \dfrac{\omega h}{X_{ac}} [-X_{ac} i_d(n) - R i_q(n) - U_{cq}(n)] \\ i_{dc}(n+1) = \dfrac{U_{cd}(n) \cdot i_d(n) + U_{cq}(n) \cdot i_q(n)}{U_{dc}(n)} \end{cases} \tag{16}$$

where ω is the AC frequency, $h$is the iteration step.

As shown in FIGURE 5, U_{dc} is updated in DC line model, which will be expressed in Section III Part E. Through the iteration of (13)(16), the transient characteristic of VSC under DC bus voltage control can be analyzed.

C. TRANSIENT MODELING OF VSC UNDER ACTIVE POWER CONTROL

In the similar way as the DC bus voltage control, the difference equations of active power control can be obtained. And the difference equations of control system outputs $U^*_{cd\_P}$ and $U^*_{cq\_P}$ under active power control can be expressed as:

$$\begin{cases} U^*_{cd\_P}(n) = u_{cd1\_P}(n) + u_{cd2\_P}(n) + u_{cd3\_P}(n) \\ U^*_{cq\_P}(n) = u_{cq1\_P}(n) + u_{cq2\_P}(n) + u_{cq3\_P}(n) \end{cases} \tag{17}$$

where the equations of u_{cq1_P}, u_{cq2_P} and u_{cq3_P} are same as u_{cq1}, u_{cq2} and u_{cq3} in (15) respectively. u_{cd1_P}, u_{cd2_P} and

u_{cd3_P} can be expressed as:

$$\begin{cases} u_{cd1\_P}(n) = -K_{p1}\cdot K_{p2}\cdot[\dfrac{\tau_{i1}\tau_{i2}k^2+(\tau_{i1}+\tau_{i2})k+1}{\tau_{i1}\tau_{i2}k^2}\cdot \\ (P_{ref}-P_{ac}(n))+\dfrac{2-2\tau_{i1}\tau_{i2}k^2}{\tau_{i1}\tau_{i2}k^2}\cdot(P_{ref}-P_{ac}(n-1)) \\ +\dfrac{\tau_{i1}\tau_{i2}k^2-(\tau_{i1}+\tau_{i2})k+1}{\tau_{i1}\tau_{i2}k^2}\cdot(P_{ref}-P_{ac}(n-2))] \\ +2u_{cd1\_P}(n-1)-u_{cd1\_P}(n-2) \\ u_{cd2\_P}(n) = K_{p2}\cdot[\dfrac{1+k\tau_{i2}}{k\tau_{i2}}\cdot i_d(n)+\dfrac{1-k\tau_{i2}}{k\tau_{i2}}\cdot i_d(n-1)] \\ +u_{cd2\_P}(n-1) \\ u_{cd3\_P}(n) = U_s(n)+X_{ac}i_q(n) \end{cases} \tag{18}$$

where P_{ref} is reactive power reference.

Meanwhile, the difference equations $U^*_{cd\_P}$ and $U^*_{cq\_P}$ also need to be processed by (3) to obtain U_{cd_P} and U_{cq_P} when the output of current controllers hits the limitation.

The control system inputs of active power control are i_d, i_q, P_s and Q_s. And the expressions of i_d, i_q, P_s and Q_s can be expressed by (16). Through the iteration of (16)(17), the transient characteristic of VSC under active power control can be analyzed.

D. VALIDATION AND COMPARISON OF VSC MODEL

The transient model of VSC proposed above should be verified and the transient characteristic of VSC under two control strategies need to be compared. The transient model of VSC shown in FIGURE 3 is taken as simulation model. And the change of i_{dc} within 10ms after fault can be obtained by the simulation, CCS equivalent model and analytical expression proposed above respectively.

The value of i_{dc} under DC bus voltage control is shown as FIGURE 6(a). According to the comparison, i_{dc} obtained by the proposed model can follow the current obtained by the simulation. For example, i_{dc} obtained by both the proposed model and simulation have an inflection point at 4.7ms.

The value of i_{dc} under active power control are shown as FIGURE 6(b). The i_{dc} waveform obtained by simulation has fluctuations while the i_{dc} waveform obtained by the proposed model is smooth. It can be found that those two waveform match well within 10ms.

The absolute error of i_{dc} under DC bus voltage control is shown as FIGURE 6(c). Since the current keeps steady until 2ms, the errors obtained by both CCS model and the proposed model are slight. The error obtained by CCS model increases quickly from 2ms to 10ms and reaches to 46.3% at 10ms. While the error obtained by the proposed model fluctuates in a small range and keeps under 2.28% all the time.

The absolute error of i_{dc} under active power control are shown as FIGURE 6(d). The error obtained by CCS model increases quickly after fault occurs and almost reaches to 59.36% at 10ms. While the error obtained by the proposed model fluctuates in a small range and keeps under 2.92% all the time.

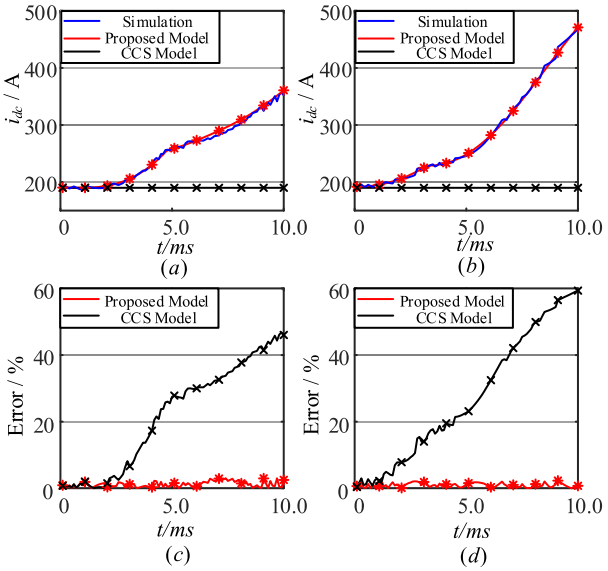

FIGURE 6. VSC output current i_{dc} under two different control: (a) comparison of i_{dc} under DC bus voltage control, (b) comparison of i_{dc} under active power control, (c) absolute error of i_{dc} under DC bus voltage control, (d) absolute error of i_{dc} under active power control.

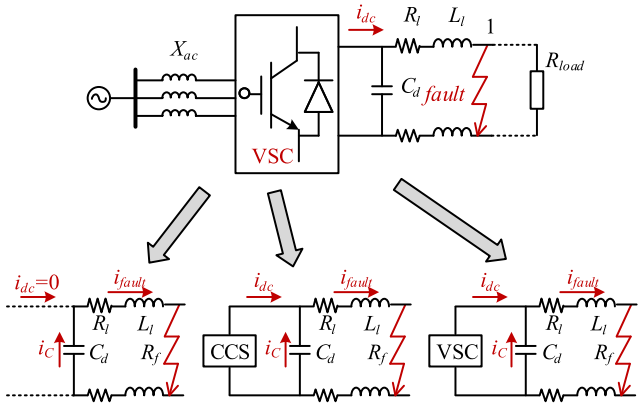

FIGURE 7. DC microgrid and equivalent topology under short circuit fault.

As shown in FIGURE 7, there are three way to calculate the injection current i_{dc} from VSC. The first way is to ignore the current from VSC. The second way is to regard the VSC as CCS. The third way is to model and analyze the transient characteristic of VSC. The fault current i_{fault} and the error of fault current obtained by different ways are shown in FIGURE 8. Both the CCS model and the proposed model are more accurate than ignoring i_{dc} from VSC. The CCS model does have similar accuracy to the proposed model in short time (4ms in this case) after the fault occurs, while the error of the CCS model increases gradually. The error of CCS model raises to 20% at 10ms and raises to 100% at 20ms. However, after considering the transient of injection current i_{dc}, the error of the proposed model can keep in 3% within 20ms.

E. DC LINE MODELING

DC line modeling is the last part of DC microgrid transient modeling. In order to analyze the transient modeling of

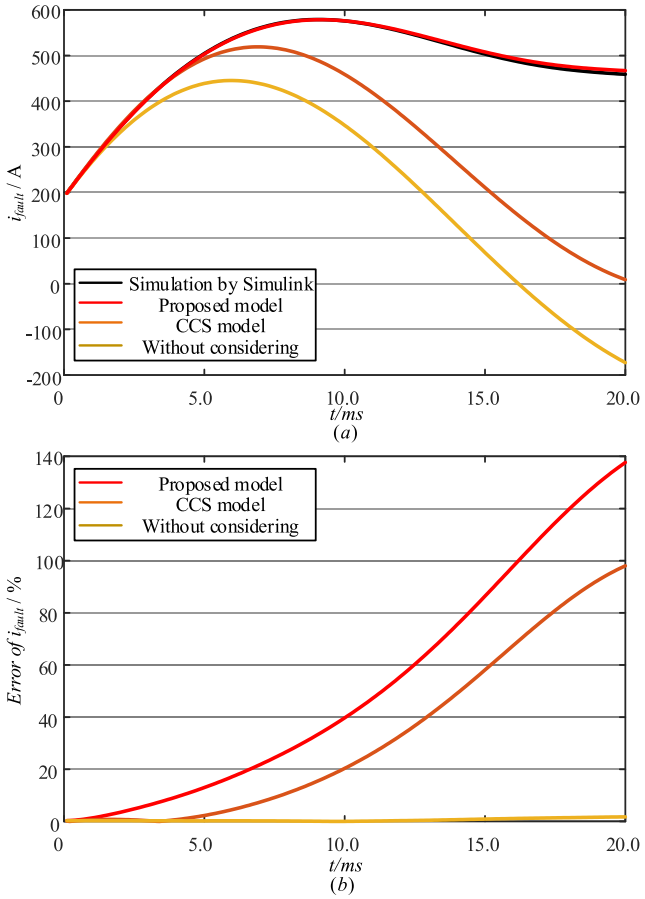

FIGURE 8. a) i_{fault} obtained by different way, b) error of i_{fault} obtained by different way.

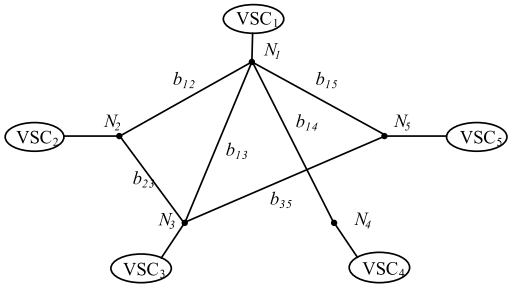

FIGURE 9. Arbitrary DC microgrid structure.

DC microgrid, an arbitrary DC microgrid structure is shown as FIGURE 9. The node N_i is connected to the VSC_i directly, and the line b_{ij} links the node N_i and node N_j.

According to [26], the state variables in DC microgrid mainly include nodes voltage and lines current. Assuming that there are N nodes and m lines in DC microgrid, the nodes voltage and lines current can be expressed as:

$$\begin{cases} f_i = \dfrac{du_i}{dt} = \left(I_{dci} - \sum_{k=1}^{N} i_{ik} \right) / C_i \\ g_l = \dfrac{di_l}{dt} = (u_a - u_b - i_l \cdot R_l) / L_l \end{cases} \tag{19}$$

where C_i is node i bus capacitance, u_i is node i voltage, I_{dci} is current from VSC to node i, i_{ik} is current from node$i$ to node k.L_l is line l inductance, R_l is line l resistance, i_l is current flowing in line l, u_a and $u_b$are node voltage at both sides of line l.

The nodes voltage and lines current can be solved by iteration, which can be expressed as:

$$\begin{cases} u_N(n+1) = u_N(n) + h \cdot f_N(n) \\ i_m(n+1) = i_m(n) + h \cdot g_m(n) \end{cases} \tag{20}$$

where $i_m(n)$ is the current on line m at time n, $u_N(n)$ is the voltage of node N at time n, h is the iteration step, $f_N(n)$ is the voltage change rate of node N at time n shown as (19), $g_m(n)$ is the current change rate of line m at time n shown as (19).

The transient analysis of DC microgrid needs to combine DC line and VSC transient analysis. The I_{dci} in (19) is i_{dc} of VSC_i in (16) updated by VSC transient model, while the DC bus voltage U_{dc} in Part A and Part B is u_m of VSC_m in (20) updated by DC line model.

The calculation method of nodes voltage and lines current are deduced in this Part. Combined with VSC analysis in Part A and Part B, a complete DC microgrid analysis process is obtained. And the transient characteristic of faulty VSC based DC microgrid can be analyzed.

IV. VALIDATIONS

The control strategies of VSC at microgrid level can be divided into master-slave control, peer-to-peer control, and hierarchical control. This paper takes master-slave control as an example to verify the developed transient model of VSC based DC microgrid in this paper. The other control strategies, which are ignored in this Section, can also use the proposed method to conduct faulty VSC based DC microgrid analysis.

A. THE FIVE-TERMINAL DC MICROGRID TEST SYSTEM

State Grid Smart Grid Research Institute (SGRI) proposed a DC grid preliminary benchmark model called DCS-M [27]. Based on DCS-A in DCS-M, a five terminal DC microgrid test system is established as shown in FIGURE 10.

There is a master unit and multiple slave units in master-slave control strategy. The master unit employs the DC bus voltage control to provide DC voltage reference, while the slave units use active power control to absorb the renewable energy. Thus, in this paper, DC bus voltage control is used in node 2 to maintain the voltage stability of DC microgrid. Power control is used in other nodes. Node 1 and 4 output active power from DC microgrid to other grids while node 3 and 5 input active power from other grids to DC microgrid.

The DC voltage of node 2 is set as 1000V. The output power of node 1 and 4 are set as 150kW respectively. The input power of node 3 and 5 are set as 100kW respectively. DC bus capacitance of each node is 8000μF. The line resistance is 0.06Ω/km. The line inductance is 0.96mH/km. The parameters of DC lines are shown in Table 1.

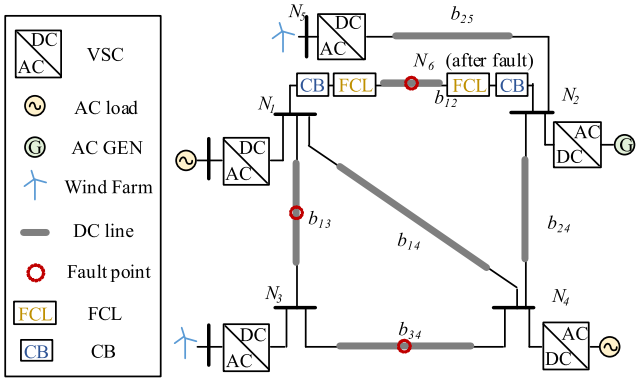

FIGURE 10. The schematic diagram of DC microgrid test system.

TABLE 1. Parameters of DC lines.

Line	Length(km)	Resistance(Ω)	Inductance(mH)
1-2	3	0.180	2.880
1-3	2.8	0.168	2.688
1-4	3.9	0.234	3.744
2-4	2.5	0.150	2.400
2-5	1.6	0.096	1.536
3-4	2.8	0.168	2.688

TABLE 2. Steady-state node voltage and line current.

Node	1	2	3	4	5	
Value(V)	967	1001.5	984	968	1020	
Line	1-2	1-3	1-4	2-4	2-5	3-4
Value(A)	-97	-54	-4.1	110	-98	48

B. VALIDATION OF PROPOSED CALCULATION METHOD

It is assumed that pole-to-pole fault occurs at the mid-point of line 1-2. The faulty point is named as node 6. The short-circuit fault is analyzed by the DC microgrid model developed in this paper, CCS based DC microgrid model (has the highest accuracy in previous references) and Matlab/Simulink simulation respectively.

1) CALCULATION ACCURACY

By calculating the steady-state power flow of the VSC based DC microgrid, the steady-state node voltage and line current can be obtained, as shown in Table 2. The fault is assumed to occur at 1s, line 1-6, 2-6, 1-3, 2-4 are four lines nearest to the faulty point, in which line 1-6 and line 2-6 connect to faulty point directly. Accordingly, the currents i_{16}, i_{26}, i_{13}, i_{24} flow on those lines are selected as typical analysis currents.

As shown in FIGURE 11, the closer the line to the faulty point, the greater the current on the line changes. Both i_{16} and i_{26}, which flow to faulty point directly, change over 1000A after 4ms. While i_{13} and i_{24}, which flow to faulty point indirectly, change less than 500A before 8ms. In order to analyze the accuracy of the method proposed in this paper, the absolute errors of faulty current calculated by the proposed model and CCS based model are shown in FIGURE 12.

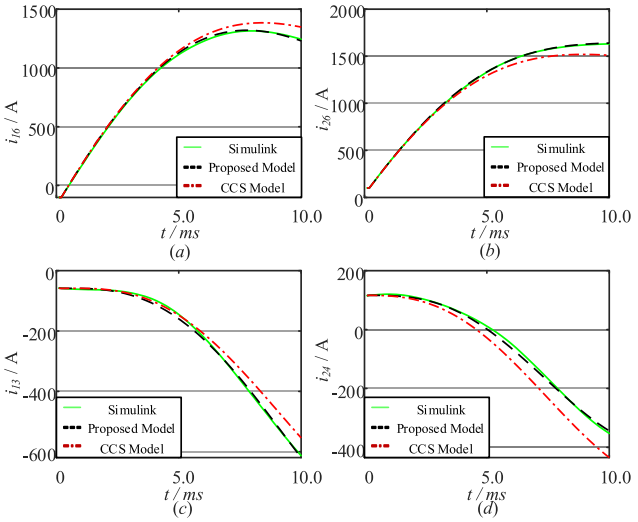

FIGURE 11. The currents obtained by Simulation and Calculation: (a) comparison of i_{16}, (b) comparison of i_{26}, (c) comparison of i_{13}, (d) comparison of i_{24}.

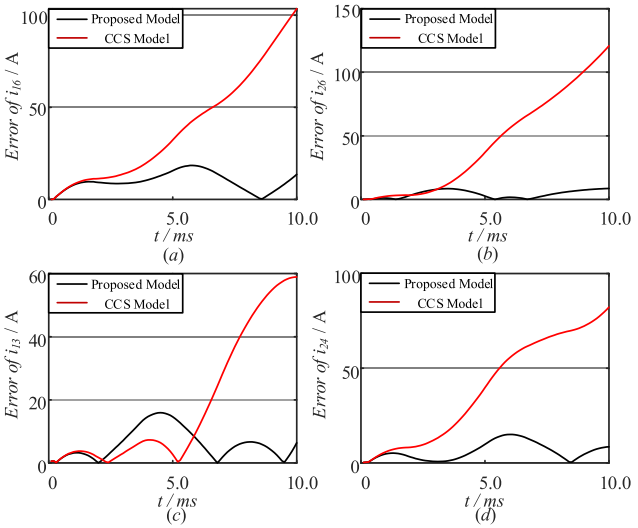

FIGURE 12. Error of typical analysis currents obtained by Simulation and Calculation: (a) error of i_{16}, (b) error of i_{26}, (c) error of i_{13}, (d) error of i_{24}.

Because the errors of i_{dc} obtained by both the proposed model and CCS based model, which are shown in FIGURE 6, are slight before 2ms. The errors of typical analysis currents i_{16}, i_{26}, i_{13}, i_{24} calculated by both the proposed model and CCS based model, which are shown in FIGURE 12, are also slight before 2ms. Because the error of i_{dc} obtained by CCS based model increases quickly from 2ms to 10ms, the errors of typical analysis currents calculated by CCS based model increases much faster than that calculated by the proposed model from 2ms to 10ms. For example, the errors of i_{16} and i_{26} calculated by CCS based model reach over 100A at 10ms. Oppositely, the errors of i_{16} and i_{26} calculated by the proposed model stay below 20A within 10ms.

According to the analysis, the CCS based model has a large error compared with simulation by Matlab/ Simulink.

TABLE 3. Calculation time under transient model and simulation.

Transient model	Simulation	Speedup factor
0.003577s	1.213410s	339.2256

While the calculated results of the proposed model are basically consistent with the simulation results. Thus, the VSC based DC microgrid model in this paper has higher calculation accuracy than the CCS based model in previous references.

2) CALCULATION EFFICIENCY

The experiment platform used in this paper is an Intel(R) core(TM) i7-8700 CPU @3.20 GHz with 16 GB RAM and a 64-bit Windows 10 Operating System. The Matlab version used in this paper is Version 9.2 (R2018b). And the Euler solver is used in Simulation. The calculation times under VSC based DC microgrid transient model and simulation are shown as Table 3.

The comparison in Table 3 shows that the transient model proposed in this paper is over 339 times faster than Simulation. Thus, the method proposed in this paper can analyze faulty DC microgrid efficiently, especially in the case that the state variables in the faulty DC microgrid need to be iterated and calculated many times, such as protection design of DC microgrid and parameters tuning of protection devices.

3) ANALYSIS OF FAULT AT OTHER LOCATION

The midpoint of line 1-3 and line 3-4 is selected as the other two fault location to further verify the accuracy of the transient modeling method. Accordingly, the currents i_{16}, i_{36}, i_{12}, i_{34} flow on those lines are selected as typical analysis currents when fault occurs in line 1-3. While the currents i_{36}, i_{46}, i_{13}, i_{24} flow on those lines are selected as typical analysis currents when fault occurs in line 3-4. The currents obtained by Simulation and Calculation are shown as FIGURE 13, FIGURE 15 respectively. While the absolute errors of faulty current calculated by the proposed model and CCS based model are shown as FIGURE 14, FIGURE 16 respectively.

As shown in FIGURE 13 and FIGURE 15, the closer the line to the faulty point, the greater the current on the line changes. Both i_{16} and i_{36} in FIGURE 13, which flow to faulty point directly, change over 1000A after 3.8ms. While i_{12} and i_{34} in FIGURE 13, which flow to faulty point indirectly, change less than 700A before 10ms. Both i_{36} and i_{46} in FIGURE 15, which flow to faulty point directly, change over 1000A after 3.7ms. While i_{13} and i_{24} in FIGURE 15, which flow to faulty point indirectly, change less than 800A before 10ms.

Similar to pole-to-pole fault at the midpoint of line 1-2, the errors of typical analysis currents calculated by CCS based model increases much faster than that calculated by the proposed model. For example, the errors of i_{16} and i_{36} in FIGURE 14 calculated by CCS based model reach around 100A at 10ms, while the errors of i_{16} and i_{36} in FIGURE 14 calculated by the proposed model stay below

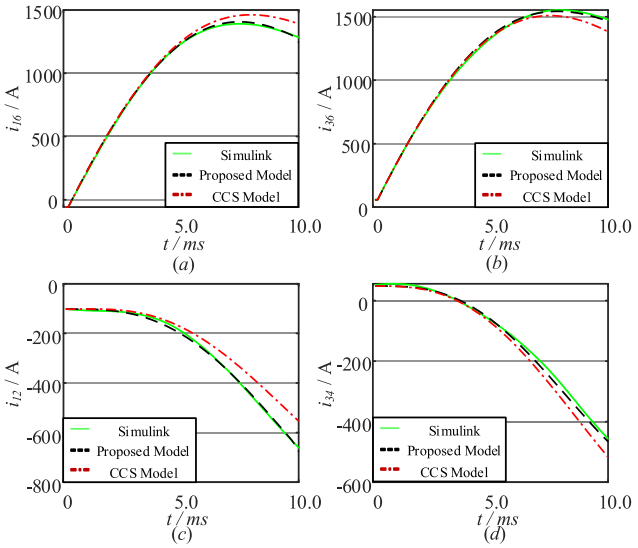

FIGURE 13. The currents obtained by Simulation and Calculation: (a) comparison of i_{16}, (b) comparison of i_{36}, (c) comparison of i_{12}, (d) comparison of i_{34}.

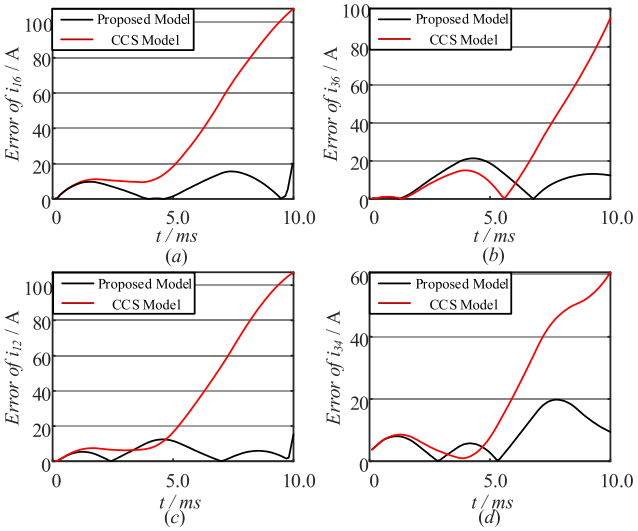

FIGURE 14. Error of typical analysis currents obtained by Simulation and Calculation: (a) error of i_{16}, (b) error of i_{36}, (c) error of i_{12}, (d) error of i_{34}.

20A within 10ms. And the errors of i_{36} and i_{46} in FIGURE 16 calculated by CCS based model reach around 100A at 10ms, while the errors of i_{36} and i_{46} in FIGURE 16 calculated by the proposed model stay below 20A within 10ms.

C. APPLICATION OF DC MICROGRID TRANSIENT MODEL

The parameters configuration of protection devices in DC microgrid is one of the most typical application for the transient modeling of DC microgrid. Moreover, CB and fault current limiter (FCL) are two mainly protection devices in faulty DC microgrid [26].Thus, in order to verify the value of the transient modeling method proposed in this paper, the method is used to analyze the transient characteristics of

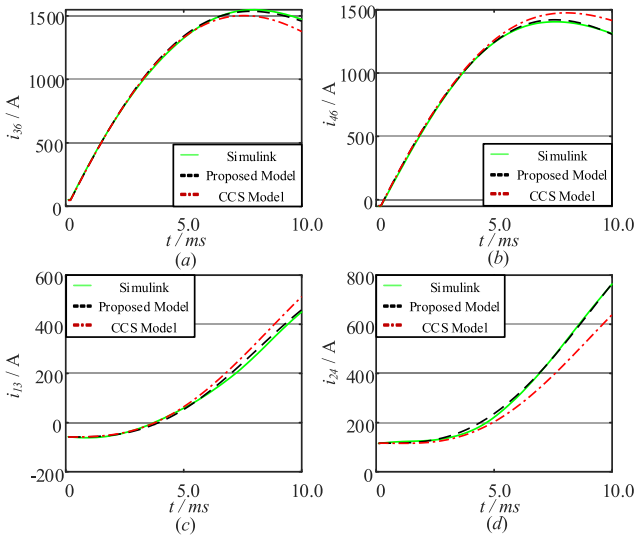

FIGURE 15. The currents obtained by Simulation and Calculation: (a) comparison of i_{36}, (b) comparison of i_{46}, (c) comparison of i_{13}, (d) comparison of i_{24}.

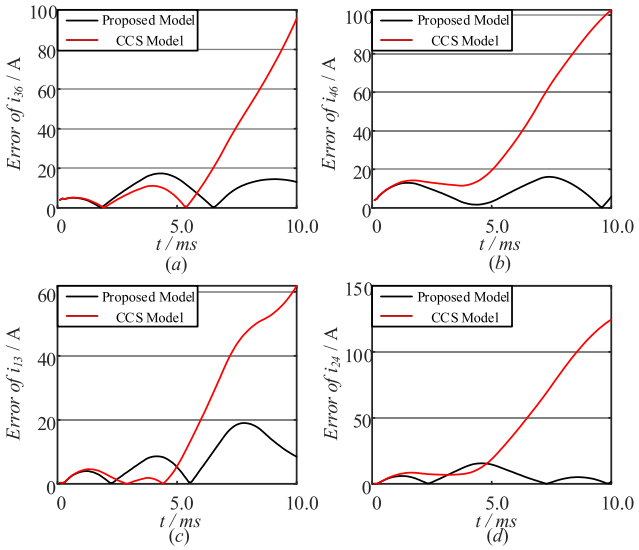

FIGURE 16. Error of typical analysis currents obtained by Simulation and Calculation: (a) error of i_{36}, (b) error of i_{46}, (c) error of i_{13}, (d) error of i_{24}.

faulty DC microgrid under different parameters of CB and FCL. And then, the parameters configuration of protection devices can be achieved based on the transient characteristics of faulty DC microgrid.

As same to Section IV Part B, the pole-to-pole fault occurs at node 6 is taken as an analysis example. As shown in FIGURE 10, the CBs and FCLs are installed at both ends of line 1-2 to limit faulty current and cutoff faulty line. The transient characteristic of faulty point current I_{fault} is relative to CB breaking time, resistance and inductance in FCL. The range of FCL resistance is assumed in [0, 2Ω]. The range of FCL inductance is assumed in [0, 20mH]. The CB breaking times are assumed at 2ms, 4ms, 6ms, 8ms. With the help of transient model in this paper, I_{fault} under different CB

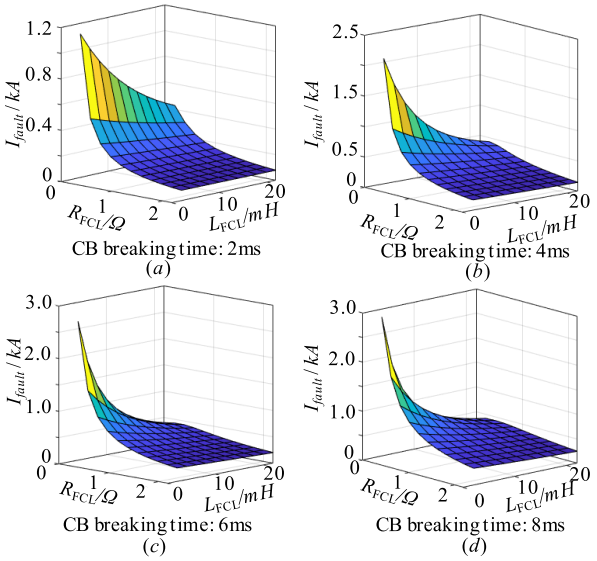

FIGURE 17. Current of line 1-6 under different CB breaking time, FCL resistance and FCL inductance.

breaking time, FCL resistance and FCL inductance can be calculated.

The transient characteristic of I_{fault} in faulty VSC based DC microgrid under different parameters of CB and FCL is shown in FIGURE 17. It can be found that the incremental rate of I_{fault} decreases when FCL is installed in line 1-2. And the limiting capacity of FCL on faulty current is non-linear. The improvement of FCL limiting capacity gradually weakens with the increase of FCL resistance or inductance. On the other hand, the smaller the CB breaking time, the less the faulty current I_{fault}. Since the incremental rate of I_{fault} decreases with time, the improvement of CB breaking time on fault current is also non-linear. Therefore, the analysis of I_{fault} proves that the method proposed in this paper can be employed to analyze the transient characteristics of VSC based DC microgrids under different system parameters.

V. CONCLUSION

This paper proposes a transient modeling method of VSC based DC microgrid. The transient characteristics of VSC under DC bus voltage control and active power control after short circuit fault occurs are analyzed in detail. Based on that, a faulty VSC based DC microgrid model is modeled and the calculation expressions of state variables are presented. The comparison of results obtained by transient model in this paper, CCS based DC microgrid model and simulation verifies the correction of approaches proposed by this paper. The method proposed in this paper has the consideration on both computational efficiency and accuracy and can be applied in various faulty DC microgrid analysis.

REFERENCES

[1] J.-D. Park, J. Candelaria, L. Ma, and K. Dunn, "DC ring-bus microgrid fault protection and identification of fault location," *IEEE Trans. Power Del.*, vol. 28, no. 4, pp. 2574–2584, Oct. 2013.

[2] J. M. Guerrero, J. C. Vasquez, J. Matas, L. G. de Vicuna, and M. Castilla, "Hierarchical control of droop-controlled AC and DC microgrids—A general approach toward standardization," *IEEE Trans. Ind. Electron.*, vol. 58, no. 1, pp. 158–172, Jan. 2011.
[3] D. Salomonsson, L. Söder, and A. Sannino, "Protection of low-voltage DC microgrids," *IEEE Trans. Power Del.*, vol. 24, no. 3, pp. 1045–1053, Jul. 2009.
[4] L. Jun, J. Tianjun, O. Gomis-Bellmunt, J. Ekanayake, and N. Jenkins, "Operation and control of multiterminal HVDC transmission for offshore wind farms," *IEEE Trans. Power Del.*, vol. 26, no. 4, pp. 2596–2604, Oct. 2011.
[5] M. P. Bahrman, J. G. Johansson, and B. A. Nilsson, "Voltage source converter transmission technologies: The right fit for the application," in *Proc. IEEE Power Eng. Soc. Gen. Meeting*, Toronto, ON, Canada, Jul. 2003, pp. 1840–1847.
[6] Z. Wang, W. Wu, and B. Zhang, "A distributed control method with minimum generation cost for DC microgrids," *IEEE Trans. Energy Convers.*, vol. 31, no. 4, pp. 1462–1470, Dec. 2016.
[7] C. N. Papadimitriou, V. A. Kleftakis, and N. D. Hatziargyriou, "A novel method for islanding detection in DC networks," *IEEE Trans. Sustain. Energy*, vol. 8, no. 1, pp. 441–448, Jan. 2017.
[8] K. Sun, K.-J. Li, Z.-D. Wang, H. Sun, M. Wang, Z. Liu, and M. Wang, "Operation modes and combination control for urban multivoltage-level DC grid," *IEEE Trans. Power Del.*, vol. 33, no. 1, pp. 360–370, Feb. 2018.
[9] G. Liu, F. Xu, Z. Xu, Z. Zhang, and G. Tang, "Assembly HVDC breaker for HVDC grids with modular multilevel converters," *IEEE Trans. Power Electron.*, vol. 32, no. 2, pp. 931–941, Feb. 2017.
[10] C. Li, C. Zhao, J. Xu, Y. Ji, F. Zhang, and T. An, "A pole-to-pole short-circuit fault current calculation method for DC grids," *IEEE Trans. Power Syst.*, vol. 32, no. 6, pp. 4943–4953, Nov. 2017.
[11] K. Satpathi, Y. M. Yeap, A. Ukil, and N. Geddada, "Short-time Fourier transform based transient analysis of VSC interfaced point-to-point DC system," *IEEE Trans. Ind. Electron.*, vol. 65, no. 5, pp. 4080–4091, May 2018.
[12] R. Mohanty and A. K. Pradhan, "DC ring bus microgrid protection using the oscillation frequency and transient power," *IEEE Syst. J.*, vol. 13, no. 1, pp. 875–884, Mar. 2019.
[13] Y. Ito, Y. Zhongqing, and H. Akagi, "DC microgrid based distribution power generation system," in *Proc. 4th Int. Power Electron. Motion Control Conf.*, Xi'an, China, vol. 3, Aug. 2004, pp. 1740–1745.
[14] S. Dhar and P. K. Dash, "Differential current-based fault protection with adaptive threshold for multiple PV-based DC microgrid," *IET Renew. Power Gener.*, vol. 11, no. 6, pp. 778–790, May 2017.
[15] W. Wang, M. Barnes, O. Marjanovic, and O. Cwikowski, "Impact of DC breaker systems on multiterminal VSC-HVDC stability," *IEEE Trans. Power Del.*, vol. 31, no. 2, pp. 769–779, Apr. 2016.
[16] A. Hassanpoor, J. Häfner, and B. Jacobson, "Technical assessment of load commutation switch in hybrid HVDC breaker," *IEEE Trans. Power Electron.*, vol. 30, no. 10, pp. 5393–5400, Oct. 2015.
[17] W. Lin and D. Jovcic, "Modelling of VSC converters in the rotating dq frame for DC fault," in *Proc. 11th IET Int. Conf. AC DC Power Transmiss.*, Birmingham, U.K., Feb. 2015, pp. 1–6.
[18] W. Lin and D. Jovcic, "Dynamic modelling of VSCs in a dq rotating frame for pole-to-pole DC fault study," *IET Gener., Transmiss. Distrib.*, vol. 11, no. 4, pp. 1072–1081, Nov. 2017.
[19] K. Wang, X. Hu, W. Sun, H. Sun, and K. Zhang, "DC voltage control and power dispatch study of a five-terminal DC grid based on average-value VSC model," in *Proc. Int. Conf. Power Syst. Technol.*, Chengdu, China, Oct. 2014, pp. 2285–2292.
[20] S. Li, W. Chen, Y. Yan, T. Shi, and C. Xia, "A multimode space vector overmodulation strategy for ultrasparse matrix converter with improved fundamental voltage transfer ratio," *IEEE Trans. Power Electron.*, vol. 33, no. 8, pp. 6782–6793, Aug. 2018.
[21] Y. Wang, W. Li, X. Wu, and X. Wu, "A novel bidirectional solid-state circuit breaker for DC microgrid," *IEEE Trans. Ind. Electron.*, vol. 66, no. 7, pp. 5707–5714, Jul. 2019.
[22] W. Li, Y. Wang, X. Wu, and X. Zhang, "A novel solid-state circuit breaker for on-board DC microgrid system," *IEEE Trans. Ind. Electron.*, vol. 66, no. 7, pp. 5715–5723, Jul. 2019.
[23] R. Lazzari and L. Piegari, "Design and implementation of LVDC hybrid circuit breaker," *IEEE Trans. Power Electron.*, vol. 34, no. 8, pp. 7369–7380, Aug. 2019.
[24] D. Keshavarzi, E. Farjah, and T. Ghanbari, "Hybrid DC circuit breaker and fault current limiter with optional interruption capability," *IEEE Trans. Power Electron.*, vol. 33, no. 3, pp. 2330–2338, Mar. 2018.
[25] C. Qian, T. Guoqing, and H. Ming, "Steady-state model and controller design of a VSC-HVDC converter based on dq0-axis," *Automat. Electr. Power Syst.*, vol. 28, no. 16, pp. 61–66, Aug. 2004.
[26] L. Kong, H. Nian, Q. Huang, Z. Zhang, J. Xu, and K. Dai, "Optimization of current breaker and fault current limiter in DC micro-grid based on faulty transient analysis," in *Proc. 21st Int. Conf. Elect. Mach. Syst. (ICEMS)*, Jeju, South Korea, Oct. 2018, pp. 2017–2022.
[27] T. An, X. Zhou, C. Han, Y. Wu, Z. He, H. Pang, and G. Tang, "A DC grid benchmark model for studies of interconnection of power systems," *CSEE J. Power Energy Syst.*, vol. 1, no. 4, pp. 101–109, Dec. 2015.

HENG NIAN (M'09–SM'14) received the B.Eng. and M.Eng. degrees from the Hefei University of Technology, China, in 1999 and 2002, respectively, and the Ph.D. degree from Zhejiang University, China, in 2005, all in electrical engineering.

From 2005 to 2007, he held a postdoctoral position at the College of Electrical Engineering, Zhejiang University, China. In 2007, he was promoted as an Associate Professor. Since 2016, he has been a Full Professor with the College of Electrical Engineering, Zhejiang University. From 2013 to 2014, he was a Visiting Scholar with the Department of Electrical, Computer, and System Engineering, Rensselaer Polytechnic Institute, Troy, NY, USA. He has published more than 20 IEEE/IET Transaction articles and holds more than 20 issued/pending patents. His current research interests include the optimal design and operation control for wind power generation systems.

LIANG KONG received the B.Eng. degree from Zhejiang University, Hangzhou, China, in 2016, where he is currently pursuing the Ph.D. degree in electrical engineering. His research interests include transient analysis and fault protection of DC microgrid.